

Flexible semi-transparent organic spin valve based on bathocuproine

Xiangnan Sun, Amilcar Bedoya-Pinto, Roger Llopis, Fèlix Casanova, and Luis E. Hueso

Citation: [Applied Physics Letters](#) **105**, 083302 (2014); doi: 10.1063/1.4894114

View online: <http://dx.doi.org/10.1063/1.4894114>

View Table of Contents: <http://scitation.aip.org/content/aip/journal/apl/105/8?ver=pdfcov>

Published by the [AIP Publishing](#)

Articles you may be interested in

[Spin-dependent transport behavior in C60 and Alq3 based spin valves with a magnetite electrode \(invited\)](#)

J. Appl. Phys. **115**, 172608 (2014); 10.1063/1.4870154

[Electron and spin transport studies of gated lateral organic devices](#)

J. Appl. Phys. **112**, 124510 (2012); 10.1063/1.4770230

[Manipulating spin injection into organic materials through interface engineering](#)

Appl. Phys. Lett. **101**, 022416 (2012); 10.1063/1.4737008

[Room-temperature organic-based spin polarizer](#)

Appl. Phys. Lett. **99**, 153503 (2011); 10.1063/1.3651329

[Planar-type spin valves based on low-molecular-weight organic materials with La 0.67 Sr 0.33 Mn O 3 electrodes](#)

Appl. Phys. Lett. **92**, 153304 (2008); 10.1063/1.2905288

The advertisement features a red and white border. On the left, text reads 'Confidently measure down to 0.01 fA and up to 10 PΩ' and 'Keysight B2980A Series Picoammeters/Electrometers'. A red button with white text says 'View video demo >'. On the right, there is an image of the Keysight B2980A device and the Keysight Technologies logo.

Flexible semi-transparent organic spin valve based on bathocuproine

Xiangnan Sun,¹ Amilcar Bedoya-Pinto,¹ Roger Llopis,¹ Fèlix Casanova,^{1,2}
 and Luis E. Hueso^{1,2,a)}

¹CIC nanoGUNE, Tolosa Hiribidea 76, 20018 Donostia San Sebastian, Spain

²IKERBASQUE, Basque Foundation for Science, 48011 Bilbao, Spain

(Received 21 July 2014; accepted 16 August 2014; published online 26 August 2014)

Organic semiconductors are attractive materials for advanced spintronic applications due to their long spin lifetimes and, simultaneously, their mechanical flexibility. With the aim of combining these advantages in a single device, we report on the fabrication and properties of a mechanically flexible bathocuproine-based spin valve. This organic spin device shows great stability on both electrical and magneto-transport properties upon mechanical bending at different radius (up to $r = 5$ mm), while featuring long-lasting endurance (on bending over 50 times). The room-temperature magnetoresistance ratio reaches up to 3.5%, and is notably preserved under air atmosphere. The observation of spin transport at room-temperature, combined with the outstanding mechanical properties and air stability, highlights the potential of bathocuproine-based spin devices towards applications. © 2014 AIP Publishing LLC. [<http://dx.doi.org/10.1063/1.4894114>]

Organic semiconductors (OSCs) have been recently attracting much interest in the field of spintronics due to their ability for transporting spin polarized carriers for long times (up to hundreds of microseconds)^{1–3} and the hybridization effects occurring at interfaces between ferromagnetic metals and molecules,^{4–6} which potentially can be exploited in device applications.^{7–9} The most basic organic spintronic device is possibly the spin valve, composed of two ferromagnetic metals (FM) separated by a non-magnetic conducting or semi-conducting organic layer, commonly used to study spin transport phenomena through the non-magnetic material.

Besides, organic materials have advantages when compared with inorganic materials in terms of their mechanical properties, impinging on their suitability to build flexible devices.¹⁰ Indeed, in the last decade, the search for flexible applications has aroused a considerable interest in the field of organic electronics, including organic field effect transistors,^{11,12} light-emitting diodes,^{13,14} memories,^{15,16} solar cells,^{17,18} sensors,^{19,20} and even smart skin.²¹

Merging both the spin and the mechanical properties of the OSC is a fairly unexplored field. Most of the existing reports so far on stretchable or bendable spin valves are based on inorganic spacer materials, such as metals^{22–24} or metal oxide tunnel barriers,^{25,26} while flexible spin devices with organic spacers have remained largely unmapped. We believe that flexible organic spintronic devices working in real operative conditions (such as room-temperature and air atmosphere) could be a particularly promising area.

In this letter, we report a flexible spin valve based on bathocuproine (BCP). BCP is a common organic semiconductor frequently employed in electronic, and more recently in spintronic applications.^{27–29} Our devices are typically composed of vertical stacks of FM/AIO_x/BCP/FM, with the important point that the AIO_x does not form a fully oxidized insulating barrier. Through this subtle difference from the mainstream metal tunnel junctions ubiquitous in literature,

we improve the mechanical properties of the device: both electrical and magneto properties of the BCP spin valves are nearly unaffected upon mechanical bending in a wide range of bending radii (r from 40 mm to 5 mm) or when bended for 50-times (even for a $r = 5$ mm). Besides the mechanical flexibility, these BCP-based spin valves have very stable magnetoresistance (MR) signal at room temperature either under vacuum or under air atmosphere (with values up to 3.5%).

Fig. 1(a) shows the cross-bar geometry of the vertical BCP-based spin valve, with a structure of Co (11 nm)/AIO_x (1.5 nm)/BCP (10 nm)/Ni₈₀Fe₂₀ (NiFe, 11 nm). The spin valve structure was deposited on a transparent poly(ethylene terephthalate) (PET) substrate through shadow mask

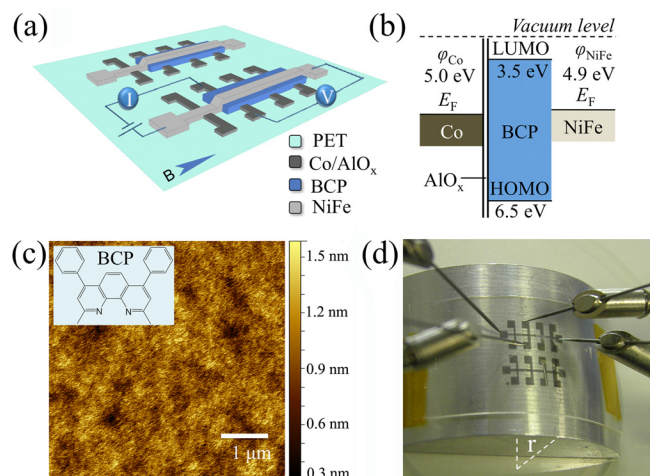


FIG. 1. (a) Schematic representation of the eight cross-bar junctions in a chip, six with BCP and two reference junctions without BCP. All the junctions have been measured using the same highlighted 4-point geometry. The arrow in this image indicates the direction of the magnetic field (B). (b) Rigid energy band diagram for the Co/AIO_x/BCP/NiFe stack. ϕ represents the work function of the metals. (c) AFM image ($5 \times 5 \mu\text{m}^2$) of a 10-nm thick BCP film deposited on PET/Co/AIO_x. The RMS roughness is 0.28 nm, and the peak-peak roughness amounts to 1.3 nm. The molecular structure of BCP is shown as inset. (d) Photograph of the 4-probe bending radius experiment. The radius of the curved supporter is used as a parameter in the device characterization.

^{a)}E-mail: l.hueso@nanogune.eu

in an ultra high vacuum (UHV) dual chamber evaporator ($p_{\text{base}} = 10^{-10}$ mbar). The metallic layers have been grown via e-beam evaporation, while the BCP molecule is evaporated using a conventional effusion cell. The AlO_x is fabricated by depositing a thin Al metal layer ($t = 1.5$ nm) and subsequent exposure to oxygen plasma. The purpose of the AlO_x layer is not to act as a tunnel barrier, hence, it is conductive (“leaky barrier”) and its properties are closer to the ones of a bad metal, so that the measured electrical and magnetotransport properties of the vertical stack are dominated by the molecular layer. It is also worth mentioning that no MR signal has been detected in the reference $\text{Co}/\text{AlO}_x/\text{NiFe}$ devices either with 4-probe or 2-probe measurement configuration.

A rigid energy map of the $\text{Co}/\text{AlO}_x/\text{BCP}/\text{NiFe}$ device is shown in Fig. 1(b). As displayed in this diagram, BCP, a typical electron-transport and hole block material, has an energetically high lowest unoccupied molecular orbital (LUMO, -3.2 eV) and a very low-lying highest unoccupied molecular orbital (HOMO, -6.5 eV). The molecular structure of BCP is shown in Fig. 1(c) as an inset image. Atomic force microscopy (AFM) has been employed to study the morphology of BCP film (see Fig. 1(c)). The root mean square (RMS) roughness of a 10-nm BCP film deposited on a PET/ Co/AlO_x stack is of just 0.28 nm (calculated across $5 \times 5 \mu\text{m}^2$ AFM images). The electrical and magneto-transport measurements were carried out using a 4-probe method to avoid the effect from contact resistances and to decrease the measurement noise (a sketch of the measurement setup is shown in Figs. 1(a) and 1(d)). In particular, Fig. 1(d) shows a photograph of the 4-probe current-voltage (I-V) measurements under a bending radius. The radius (labelled as r in Fig. 1(d)) of the curved supporter is used as a parameter to describe the bending radius in the device characterization. In our experiments, six samples (same to Figs. 1(a) and 1(d)) have been fabricated with the same fabrication recipe, making a total of 36 BCP-based junctions and 12 reference junctions. Among

those samples, more than 70% of the BCP-based devices exhibit MR signal.

The photographs of the flexible semi-transparent BCP-based devices are shown in Fig. 2(a) together with the curved supports employed for the non-planar electrical transport measurements (with radius from 5 to 40 mm). The current (I)-voltage (V) curves of the $\text{Co}/\text{AlO}_x/\text{BCP}/\text{NiFe}$ devices under different bending conditions are shown in Fig. 2(b). There is no change in the I-V characteristics when the device is placed either planar or bended at different angles. Fig. 2(c) shows the I-V measurements as a function of bending time, demonstrating that the electrical properties of the devices remain unaffected after 50-times bending ($r = 5$ mm). The stability of the I-V curves, even when the devices are bended multiple times to such a small radius (5 mm), is a property that has not been yet achieved in inorganic flexible spin devices.^{24–26}

Besides the BCP-based devices, fully inorganic $\text{Co}/\text{Al}_2\text{O}_3/\text{NiFe}$ magnetic tunnel junctions (MTJs) have been fabricated as a reference for comparing the mechanical properties. In this case, the Al_2O_3 layer employed is a standard fully oxidized layer which acts as a tunnel barrier, quite differently from the leaky AlO_x layer used in the $\text{Co}/\text{AlO}_x/\text{BCP}/\text{NiFe}$ device. The inorganic MTJs show very limited mechanical flexibility, as the devices become much more conductive or even short circuited (with resistance values typical of a Co/NiFe junction between 200 Ω and 1 k Ω in 2-point, less than 100 m Ω in 4-point measurements) after just one bending process (see Fig. 2(d)), presumably due to crack formation at such high stress load. We should mention that the I-V properties of the Co and NiFe electrodes in both $\text{Co}/\text{AlO}_x/\text{BCP}/\text{NiFe}$ and $\text{Co}/\text{Al}_2\text{O}_3/\text{NiFe}$ devices do not display any change after mechanical bending. Then, it is clear that the combination of the AlO_x leaky barrier and the BCP as molecular spacer exhibits highly improved mechanical properties compared to our fully inorganic spin valves.

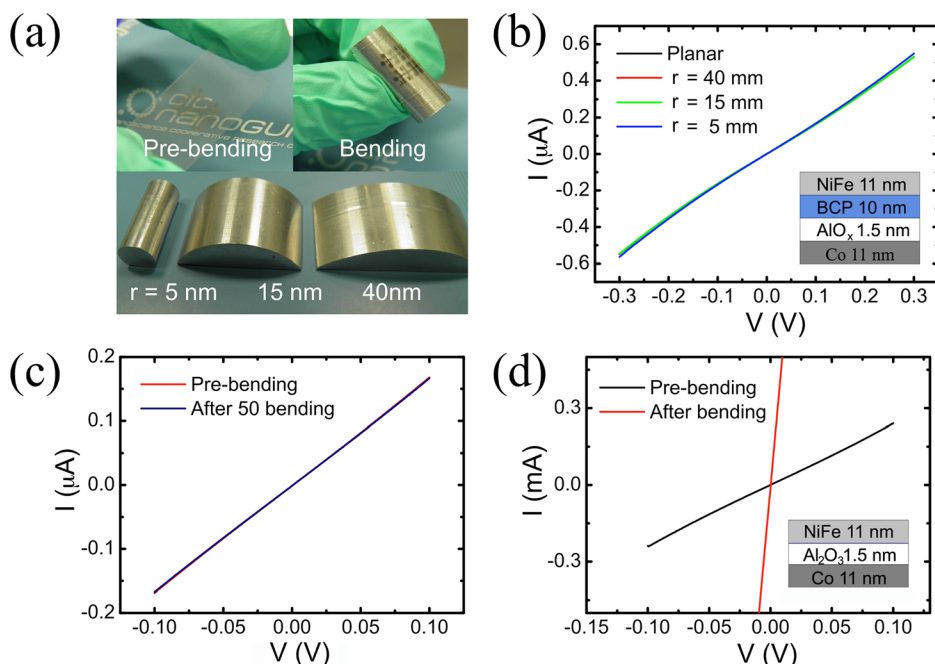


FIG 2. (a) Photographs of the flexible semi-transparent BCP based spin valve, the bending-tolerance test, and the curved supports employed in this work ($r = 5$ mm, 15 mm, and 40 mm, respectively, from left to right). (b) and (c) I-V measurements of BCP based spin-valve on PET substrate as a function of bending radius and bending time ($r = 5$ mm). (d) I-V measurements of an inorganic reference $\text{Co}/\text{Al}_2\text{O}_3/\text{NiFe}$ device before and after bending ($r = 5$ mm). All the I-V curves shown in this figure are measured without light exposure, at room-temperature and under vacuum.

Besides the electrical transport characteristics, the magnetoresistance of the BCP-based devices has also been studied. The MR measurements are carried out with a 4-probe method at a low injection bias (0.01 V), at room temperature, under vacuum and without light exposure. The average room-temperature MR of a 10-nm BCP based spin valve is 3% (value averaged among six chips), with a maximum MR up to 3.5%. This value is only slightly lower than the ones measured in devices fabricated on a SiO₂ substrate.²⁹ Fig. 3(a) shows the MR measurements of the BCP spin valve as a function of the bending radius. We can observe how both the shape of the MR curve and the value of the MR ratio are nearly constant in the range from 40 mm to 5 mm bending radii. Fig. 3(b) shows the bending tolerance tests of the BCP-based spin valve. Both the MR shape and value remain almost constant after bending for 50 times, demonstrating the excellent stability and endurance of the flexible devices.

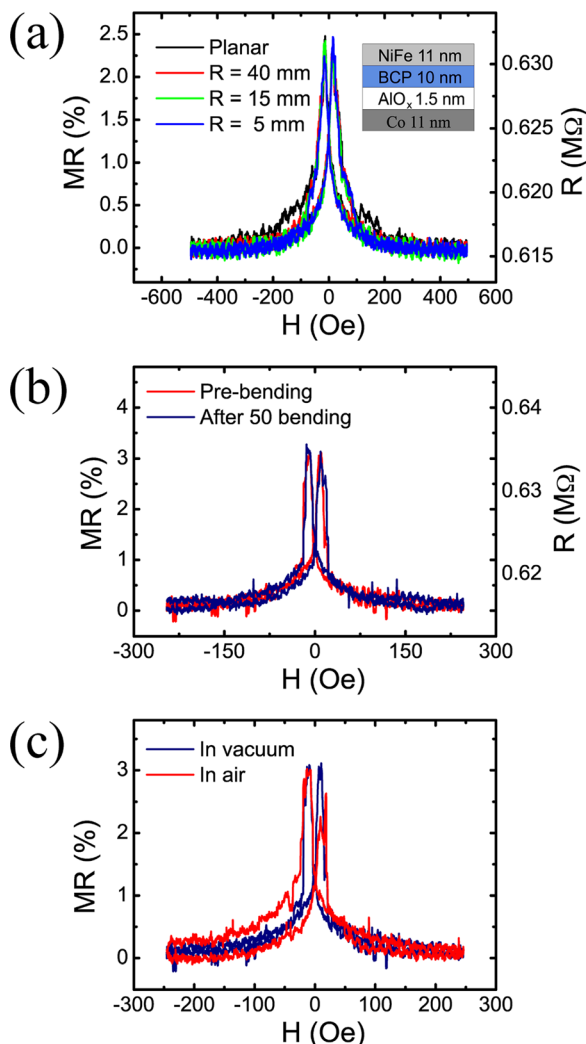


FIG. 3. MR measurements of flexible BCP-based spin valves. (a) MR as a function of bending radius. (b) Change in the MR properties with the number of bending processes. The curves shown in (a) and (b) are measured with different devices from different chips. The resistances labelled in (a) and (b) correspond to the curves of “Planar” and “Pre-bending” states, respectively. (c) MR under different ambient conditions (under vacuum or in air). All the MR measurements shown in this figure are carried out in the dark and at room-temperature. All the devices measured in this figure have the same structure as shown in (a).

Since the measured currents are in nA-scale, any change in the device conductance induced by mechanical damage or cracks in the device layers (either in the metal electrodes, the BCP spacer and/or the leaky AlO_x barrier) would be easily detected. Furthermore, mechanical damage would have an immediate impact on the spin transport and hence on the magnitude and shape of the MR signals. The constant MR curves, displayed in Figs. 3(a) and 3(b), once again demonstrate the excellent performance and robustness of the Co/AlO_x/BCP/NiFe devices under mechanical stress. Compared with previous reports on inorganic bendable spin valves (for bending radius of 10 mm),^{24–26} our BCP based spin valves exhibited nearly unaffected MR signals at a higher bending radius (up to 5 mm). On top of the excellent mechanical flexibility, the BCP-based devices retained the spin transport properties under air atmosphere (see Fig. 3(c)), similar to what has been observed on BCP spin valves grown on SiO₂ substrates.²⁹

In summary, mechanically flexible semi-transparent spin valves based on bathocuproine molecules have been fabricated. The values of room temperature MR of these devices reach up to 3.5%. Taking into account the bending radius and the bending time endurance measurements, the BCP-based devices show mechanical stability in terms of electrical and magneto-transport properties. Both the I-V and the MR characteristics are nearly invariant at different bending radius and upon bending for 50-times (up to a bending radius of 5 mm). Besides, we also observe stable room-temperature spin transport in the Co/AlO_x/BCP/NiFe devices under air atmosphere. Considering all these properties (room-temperature MR, excellent mechanical flexibility and air-stable spin transport), molecular spin valves based on BCP appear very promising for flexible spintronic applications.

This work was supported by the European Union 7th Framework Programme under the Marie Curie Actions (256470-ITAMOSINOM), NMP Project (263104-HINTS) and the European Research Council (257654-SPINTROS), and by the Spanish MINECO under Project No. MAT2012-37638.

¹S. Pramanik, C.-G. Stefanita, S. Patibandla, S. Bandyopadhyay, K. Garre, N. Harth, and M. Cahay, *Nat. Nanotechnol.* **2**, 216–219 (2007).

²V. Dediu, L. E. Hueso, I. Bergenti, and C. Taliani, *Nat. Mater.* **8**, 707–716 (2009).

³Y. Zheng and F. Wudl, *J. Mater. Chem. A* **2**, 48–57 (2014).

⁴C. Barraud, P. Seneor, R. Mattana, S. Fusil, K. Bouzehouane, C. Deranlot, P. Graziosi, L. Hueso, L. Bergenti, V. Dediu, F. Petroff, and A. Fert, *Nat. Phys.* **6**, 615–620 (2010).

⁵N. Atodiresei, J. Brede, P. Lazić, V. Caciuc, G. Hoffmann, R. Wiesendanger, and S. Blügel, *Phys. Rev. Lett.* **105**, 066601 (2010).

⁶K. V. Raman, A. M. Kamerbeek, A. Mukherjee, N. Atodiresei, T. K. Sen, P. Lazić, V. Caciuc, R. Michel, D. Stalke, S. K. Mandal, S. Blügel, M. Münzenberg, and J. S. Moodera, *Nature* **493**, 509–513 (2013).

⁷V. Dediu, M. Murgia, F. C. Maticotta, C. Taliani, and S. Barbanera, *Solid State Commun.* **122**, 181–184 (2002).

⁸Z. H. Xiong, D. Wu, Z. V. Vardeny, and J. Shi, *Nature* **427**, 821–824 (2004).

⁹S. Sanvito, *Chem. Soc. Rev.* **40**, 3336–3355 (2011).

¹⁰S. Logothetidis, *Mater. Sci. Eng. B* **152**, 96–104, (2008).

¹¹G. H. Gelinck, H. E. A. Huitema, E. van Veenendaal, E. Cantatore, L. Schrijnemakers, J. B. P. H. van der Putten, T. C. T. Geuns, M. Beenhakkers, J. B. Giesbers, B. H. Huisman, E. J. Meijer, E. M. Benito,

- F. J. Touwslager, A. W. Marsman, B. J. E. van Rens, and D. M. de Leeuw, *Nat. Mater.* **3**, 106–110 (2004).
- ¹²T. Sekitani, U. Zschieschang, H. Klauk, and T. Someya, *Nat. Mater.* **9**, 1015–1022 (2010).
- ¹³A. N. Krasnov, *Appl. Phys. Lett.* **80**, 3853 (2002).
- ¹⁴Z. B. Wang, M. G. Helander, J. Qiu, D. P. Puzzo, M. T. Greiner, Z. M. Hudson, S. Wang, Z. W. Liu, and Z. H. Lu, *Nat. Photonics* **5**, 753–757 (2011).
- ¹⁵R. H. Kim, H. J. Kim, I. Bae, S. K. Hwang, D. B. Velusamy, S. M. Cho, K. Takaishi, T. Muto, D. Hashizume, M. Uchiyama, P. André, F. Mathevet, B. Heinrich, T. Aoyama, D. E. Kim, H. Lee, J. C. Ribierre, and C. Park, *Nat. Commun.* **5**, 3583 (2014).
- ¹⁶T. Sekitani, T. Yokota, U. Zschieschang, H. Klauk, S. Bauer, K. Takeuchi, M. Takamiya, T. Sakurai, and T. Someya, *Science* **326**, 1516–1519 (2009).
- ¹⁷J. Wang, W. Weng, M. Y. Tsai, M. Lee, S. Horng, T. Perng, C. Kei, C. Yuc, and H. Meng, *J. Mater. Chem.* **20**, 862–866 (2010).
- ¹⁸M. Kaltenbrunner, M. S. White, E. D. Glowacki, T. Sekitani, T. Someya, N. S. Sariciftci, and S. Bauer, *Nat. Commun.* **3**, 770 (2011).
- ¹⁹T. Someya, Y. Kato, T. Sekitani, S. Iba, Y. Noguchi, Y. Murase, H. Kawaguchi, and T. Sakurai, *Proc. Natl. Acad. Sci.* **102**, 12321–52005 (2005).
- ²⁰Y. Noguchi, T. Sekitani, and T. Someya, *Appl. Phys. Lett.* **89**, 253507 (2006).
- ²¹T. Someya, T. Sekitani, S. Iba, Y. Kato, H. Kawaguchi, and T. Sakurai, *Proc. Natl. Acad. Sci.* **101**, 9966–9970 (2004).
- ²²M. Melzer, D. Makarov, A. Calvimontes, D. Karnaushenko, S. Baunack, R. Kaltofen, Y. Mei, and O. G. Schmidt, *Nano Lett.* **11**, 2522 (2011).
- ²³M. Melzer, G. Lin, D. Makarov, and O. G. Schmidt, *Adv. Mater.* **24**, 6468 (2012).
- ²⁴D. Karnaushenko, D. Makarov, C. Yan, R. Streubel, and O. G. Schmidt, *Adv. Mater.* **24**, 4518 (2012).
- ²⁵C. Barraud, C. Deranlot, P. Seneor, R. Mattana, B. Dlubak, S. Fusil, K. Bouzehouane, D. Deneuve, F. Petroff, and A. Fert, *Appl. Phys. Lett.* **96**, 072502 (2010).
- ²⁶A. Bedoya-Pinto, M. Donolato, M. Gobbi, L. E. Hueso, and P. Vavassori, *Appl. Phys. Lett.* **104**, 062412 (2014).
- ²⁷H. Gommans, B. Verreet, B. P. Rand, R. Muller, J. Poortmans, P. Heremans, and J. Genoe, *Adv. Funct. Mater.* **18**, 3686–3691 (2008).
- ²⁸A. P. Kulkarni, C. J. Tonzola, A. Babel, and S. A. Jenekhe, *Chem. Mater.* **16**, 4556–4573 (2004).
- ²⁹X. Sun, M. Gobbi, A. Bedoya-Pinto, O. Txoperena, F. Golmar, R. Llopis, A. Chuvilin, F. Casanova, and L. E. Hueso, *Nat. Commun.* **4**, 2794 (2014).